ON TWO OPTIMAL CONTROL PROBLEMS FOR MAGNETIC FIELDS [*]

SERGE NICAISE[†], SIMON STINGELIN[‡], AND FREDI TRÖLTZSCH[§]

Abstract. Two optimal control problems for instationary magnetization processes are considered in 3D spatial domains that include electrically conducting and nonconducting regions. The magnetic fields are generated by induction coils. In the first model, the induction coil is considered as part of the conducting region and the electrical current is taken as control. In the second, the coil is viewed as part of the nonconducting region and the electrical voltage is the control. Here, an integro-differential equation accounts for the magnetic induction law that couples the given electrical voltage with the induced electrical current in the induction coil.

We derive first-order necessary optimality condition for the optimal controls of both problems. Based on them, numerical methods of gradient type are applied. Moreover, we report on the application of model reduction by POD that lead to tremendous savings. Numerical tests are presented for academic 3D geometries but also for a real-world application.

AMS subject classification. 49K20,49M05,35K565,78A25

Key words. Evolution Maxwell equations, vector potential formulation, induction law, degenerate parabolic equation, optimal control, adjoint equation, numerical solution, model reduction, proper orthogonal decomposition

1. Introduction. In this paper, we deal with different problems of optimal magnetization that arise from applications in flow measurement. We consider the following situation: An electrically conducting tube is surrounded by an induction coil that generates a magnetic field. Applying an appropriate electrical current or voltage in the coil, the magnetic field should be influenced in an optimal way. The aim of optimization is to switch very fast from a given magnetic field to one with opposite polarization. For the modeling of the underlying application, we refer to [18].

We model the magnetization process by two different linear parabolic-elliptic evolution Maxwell systems, where the real quantity of interest, the magnetic induction B is represented by a vector potential as $B = \operatorname{curl} y$. The vector potential y is the state of our control systems. In the first problem, the electrical current is the control function that appears in the right-hand side of the evolution equation. In the second, the voltage is taken as control. To obey the induction law, this eventually leads to a controlled Maxwell integro-differential system for the state function y.

The optimal control theory of Maxwell equations became quite active in the last years. In particular, the optimal control of processes of magneto-hydrodynamics (MHD) has a fairly long tradition. Here, the control system includes Maxwell equations coupled with equations accounting for fluid flow and/or heat conduction. We mention [4], [8], [10], [6], [7], or [11] and further references cited therein.

In these papers, the Maxwell equations are posed in a steady state or time-harmonic setting, while the Navier-Stokes equations for the fluid flow are considered in a time variant setting. The time harmonic approach is also used in [14], [23],[24], [17], [5], [9].

[†]LAMAV and FR CNRS 2956, Université de Valenciennes et du Hainaut Cambrésis, Institut des Sciences et Techniques de Valenciennes, F-59313 - Valenciennes Cedex 9 France (Serge.Nicaise@univ-valenciennes.fr).

[‡]ZHAW School of Engineering, Institut für Angewandte Mathematik und Physik (IAMP), Technikumstrasse 9, Postfach, 8401 Winterthur, Switzerland (stiw@flowtec.endress. com).

[§]Institut für Mathematik, Technische Universität Berlin, D-10623 Berlin, Germany (troeltzsch@math.tu-berlin.de).

In the papers mentioned above, the Maxwell equations are coupled with the Navier-Stokes or heat equation. In contrast to them, [14] deals with the optimal control of magnetic fields in a time-harmonic setting of the Maxwell equations. In this context, we also mention the recent PhD thesis [13]. These two papers are closer to our model than the problems of coupled systems appearing in MHD control. However, in contrast to the references cited above, our two problems of optimal magnetization are modeled by evolution Maxwell equations of degenerate parabolic type. To our best knowledge, optimal control problems of this type of equations were not yet discussed in literature.

Our paper contains the following main novelties: In the analysis, we derive first-order necessary optimality conditions for two different optimal control problems for evolution Maxwell equations, in particular for a Maxwell integro-differential system. Here, we rely on the paper [19] on existence and uniqueness theorems for the state systems under consideration. We prove optimality conditions by introducing adjoint states as a basis for computational optimization techniques.

In the second part of the paper, we apply the optimality conditions to set up numerical methods. We solve problems of optimal magnetization in 3D spatial domains by gradient type methods. The computed optimal magnetization curves turned out to be very precise and are used in practical applications. Moreover, we briefly report on the application of model reduction by standard proper orthogonal decomposition (POD) that enabled us to achieve tremendous savings of computing times. A detailed discussion of model reduction, complemented by a discussion of necessary optimality conditions for a quadratic objective functional that measures the distance of $B = \operatorname{curl} y$ to a desired magnetic field, is contained in our paper [18]. We also mention the contribution [20] on the successful application of POD to the optimal control of Maxwell equations. Moreover, we refer to the recent PhD thesis by Altmann [2], who numerically determined some optimal solutions to our optimal magnetization problem.

2. Two models for magnetic fields.

2.1. The evolution Maxwell equations. The application of optimal control methods to the magnetization processes we have in mind are considered in a bounded spatial domain $\Omega \subset \mathbb{R}^3$ that stands for the "holdall domain" for the whole process. In our test examples, Ω is a cube that is taken so large that a further extension does not really change the numerical results. This domain Ω is the union of the electrically conducting domain Ω_1 and the electrically nonconducting domain Ω_2, more precisely,

$$\bar{\Omega} = \bar{\Omega}_1 \cup \bar{\Omega}_2.$$

We denote by $\Gamma := \bar{\Omega}_1 \cap \bar{\Omega}_2$ the interface between the conducting and nonconducting region and by $\nu : \partial\Omega \to \mathbb{R}^3$ the vector field of the outer unit normal on $\partial\Omega$. We shall specify the concrete geometric assumptions on these subdomains below.

Our main quantity of interest is the magnetic induction $B : \bar{\Omega} \to \mathbb{R}^3$. Thanks to the assumption that B is divergence free, we are justified to represent B by a vector potential $y : \bar{\Omega} \to \mathbb{R}^3$, namely $B := \operatorname{curl} y$. Inserting y in the standard Maxwell equations and neglecting the term $\varepsilon \, \partial^2 y/\partial t^2$, since ε is very small in our application, we finally arrive at evolution Maxwell equations of the form

$$\begin{cases} \sigma(x)\dfrac{\partial y}{\partial t}(x,t) + \operatorname{curl}\mu^{-1}\operatorname{curl} y(x,t) & = & f(x,t) & \text{in} & \Omega \times (0,T) \\ y(x,t) \times \nu & = & 0 & \text{on} & \partial\Omega \times (0,T) \\ y(x,0) & = & y_0(x) & \text{in} & \Omega_1. \end{cases} \qquad (2.1)$$
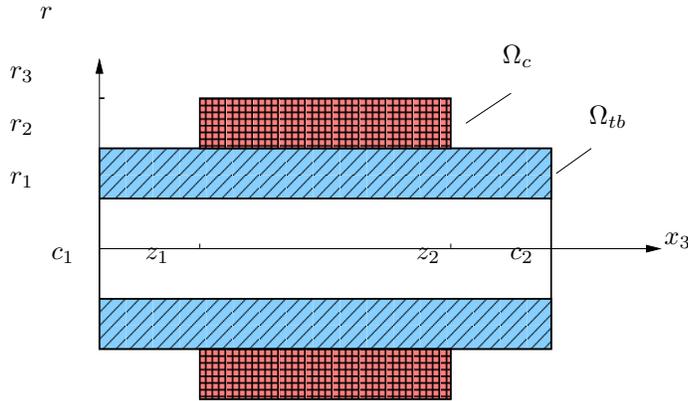
2

FIG. 2.1. *Scheme of the tube with coil – cut through the origin along the x_3-axis*

Depending on the concrete model, we will specify the given functions $f : \Omega \times (0, T) \to \mathbb{R}^3$ and $y_0 : \Omega_1 \to \mathbb{R}^3$ later. The *electrical conductivity* $\sigma : \Omega \to \mathbb{R}$ is given with some constant $\sigma_0 > 0$ by

$$\sigma(x) := \begin{cases} \sigma_0 & \text{in} \quad \Omega_1 \\ 0 & \text{in} \quad \Omega_2, \end{cases}$$

while the *magnetic permeability* $\mu : \Omega \to \mathbb{R}$ is assumed to be bounded and measurable and uniformly positive such that

$$\mu(x) \geq \mu_0 > 0 \quad \text{for a.a. } x \in \Omega.$$

In view of our computational examples, we fix the following geometry of Ω_1 and Ω_2: We have a tube Ω_{tb},

$$\Omega_{tb} = \{x \in \mathbb{R}^3 : 0 < r_1 < x_1^2 + x_2^2 < r_2, \; z_1 < x_3 < z_2\}$$

and an induction coil

$$\Omega_c = \{x \in \mathbb{R}^3 : 0 < r_2 < x_1^2 + x_2^2 < r_3, \; c_1 < x_3 < c_2\}.$$

In this setting, $r_3 > r_2$ and $z_1 \leq c_1 < c_2 \leq z_2$ are given real numbers.

Let the holdall domain $\Omega \subset \mathbb{R}^3$ be an open cube that contains $\bar{\Omega}_{tb} \cup \bar{\Omega}_c$. In both models we discuss in our paper, the tube Ω_{tb} belongs to the conducting region, while the meaning of Ω_c changes: In the first model, Ω_c is considered as part of the conducting region, hence $\Omega_1 = \text{int}\,(\bar{\Omega}_{tb} \cup \bar{\Omega}_c)$. In the second, it is modeled as nonconducting, hence $\Omega_1 = \Omega_{tb}$ and $\Omega_2 = \Omega \setminus \bar{\Omega}_{tb}$.

REMARK 1. *Our theory is also true for the following more general setting: Here, Ω, Ω_1, Ω_2, and Ω_c are (open) bounded Lipschitz domains such that $\bar{\Omega}_1 \subset \Omega$ (i.e. Ω_1 is strictly included in Ω), Ω_2 has exactly one hole formed by $\bar{\Omega}_1$ and that the boundary $\partial \Omega_2$ is composed of two connected components. We either have $\Omega_c \subset \Omega_1$ or $\Omega_c \subset \Omega_2$.*

3

2.2. Electrical current as control.

2.2.1. The control problem and its well-posedness. In our first optimal control model, we consider the electrical current as the control function. This is not very realistic, since it is mainly the voltage that can be controlled. However, this setting is simpler so that theory and numerical treatment are easier than in the second model, where the magnetic field is controlled by the voltage.

In this section, we consider the induction coil as part of the conducting region, hence here we have

$$\Omega_1 := \text{int}\,(\bar{\Omega}_{tb} \cup \bar{\Omega}_c), \quad \Omega_2 := \Omega \setminus \bar{\Omega}_1.$$

An induction coil is composed of many windings of a conducting wire so that the direction of the electrical current is given very precisely by the direction of the wire. Computing the electrical current by the Maxwell equations would be very complicated. The reason is that a finite element mesh should be extremely fine to match the geometry of the windings and empty space between them; cf. Fig. 2.2 that shows a cross section through a coil and the finite element mesh needed for computing the magnetic field. Therefore, we use the following ansatz for modeling the electrical current density j_c,

$$j_c(x,t) := e(x)\,i(t).$$

Here $i : [0,T] \to \mathbb{R}$ is the amplitude of the electrical current in one single winding and

$$e(x_1, x_2, x_3) = \begin{cases} \dfrac{N_c}{|\omega_c|\sqrt{x_1^2 + x_2^2}} \begin{bmatrix} -x_2 \\ x_1 \\ 0 \end{bmatrix} & \text{in } \Omega_c \\ 0 & \text{else,} \end{cases} \tag{2.2}$$

where N_c is a positive constant and $|\omega_c|$ is the area of a vertical cross section through the windings. In the geometry "tube with coil", the cross section ω_c is displayed as the upper red part of Fig. 1. Note that e is divergence free in the whole domain Ω.

REMARK 2. *The ansatz (2.2) for the current density can be justified as follows. The direction of the current in any point x of the coil is very well approximated by $(-x_2, x_1, 0)/\sqrt{x_1^2 + x_2^2}$, if the number of windings is large. This motivates the direction of the vector e. The factor $N_c/|\omega_c|$ has the following reason:*

Let a coil be totally filled by a wire of rectangular cross section so that no space is left between its windings. If the strength of the electrical current in the wire is $|i|$, then the total flow of the current through the cross section ω_c is $N_c\,|i|$. The ansatz (2.2) ensures in this case that the integral of the current density $e\,i$ over ω_c is just $N_c\,|i|$. In a real coil, there is some empty space between the windings that is fairly small. Here, (2.2) yields a very good approximation.

In the first model, we consider the following state equation for the vector potential y:

$$\begin{cases} \sigma_0 \dfrac{\partial y}{\partial t}(x,t) + \operatorname{curl} \mu^{-1} \operatorname{curl} y(x,t) &=& e(x)i(t) & \text{in} & \Omega_1 \times (0,T) \\ \operatorname{curl} \mu^{-1} \operatorname{curl} y(x,t) &=& 0 & \text{in} & \Omega_2 \times (0,T) \\ y(x,t) \times \nu &=& 0 & \text{on} & \partial\Omega \times (0,T) \\ y(x,0) &=& y_0(x) & \text{in} & \Omega_1. \end{cases} \tag{2.3}$$
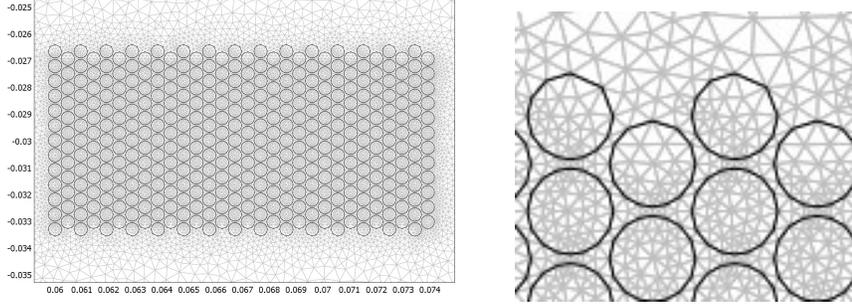
FIG. 2.2. *Windings of the coil and FE mesh*

Moreover, we shall always assume the gauging condition

$$\operatorname{div} y = 0 \text{ in } \Omega_1 \cup \Omega_2. \tag{2.4}$$

The vector function y is the *state* of our control system while i is the *control.* Notice that we cannot guarantee that y is divergence free in the whole domain Ω, since the normal component of y can be discontinuous across the interface Γ. We will include (2.4) by the choice of the state space. In what follows, we use the notation $Q_j := \Omega_j \times (0,T)$, $j = 1,2$.

The aim of our first optimal control problem is to minimize the objective functional

$$J(y,i) := \frac{\lambda_T}{2} \int_{\Omega_1} |y(x,T) - y_T(x)|^2 \, dx + \frac{\lambda_Q}{2} \iint_{Q_1} |y(x,t) - y_Q(x,t)|^2 \, dxdt + \frac{\lambda_i F}{2} \int_0^T i^2(t) \, dt, \tag{2.5}$$

where λ_T, λ_Q, and λ_i are nonnegative constants (not all being zero) and $y_Q \in L^2(Q_1)^3$ and $y_T \in L^2(\Omega_1)^3$ are given functions.

In our concrete application, we aim at switching in shortest time between two magnetic fields of opposite polarization, i.e. starting from some B_0 we want to reach $-B_0$ in short time. In the context of the vector potential, we start with y_0 and want to match $-y_0$ very fast. In this concrete example, we set $y_T(x) := -y_0(x)$ and also $y_Q(x,t) := -y_0(x)$. Here, the first part of J, weighted by λ_T, drives $y(T)$ to $-y_0$. The second part, weighted by λ_Q, accounts for the speed of this approximation. Some experience is needed to find a good balance between the parameters λ_Q and λ_T to achieve the goal of fast switching. We refer to the paper [3], where the time-optimal control of electrical circuits was discussed in this way. Notice that we do not consider the problem of reaching a given state y_T exactly, because this would rise difficult problems of exact controllability.

Next, we introduce some function spaces. We use the standard Sobolev spaces $H(\operatorname{curl}, \mathcal{O})$ and $H(\operatorname{div}, \mathcal{O})$ and the space

$$H(\operatorname{div} = 0, \mathcal{O}) := \{ y \in L^2(\mathcal{O})^3 : \operatorname{div} y = 0 \text{ in } \mathcal{O} \},$$

the space of divergence free vector functions equipped with the inner product of $L^2(\mathcal{O})^3$. It is well known that this is a Hilbert space. We also need the space

$$H_0(\operatorname{curl}, \Omega) := \{ y \in L^2(\Omega)^3 : \operatorname{curl} y \in L^2(\Omega)^3 \text{ and } y \times \nu = 0 \text{ on } \partial\Omega \}.$$

5

As state space for our problem, we define

$$Y(\Omega) := \{v \in H_0(\mathrm{curl}, \Omega) \, : \, \mathrm{div}\, v_{|\Omega_j} \in L^2(\Omega_i)^3, \ j = 1, 2, \ \text{and} \ \langle v_{|\Omega_2} \cdot \nu, 1\rangle_\Gamma = 0\}.$$

Here, $\langle \cdot, \cdot \rangle_\Gamma$ denotes the pairing between $H^{-1/2}(\Gamma)$ and $H^{1/2}(\Gamma)$. Moreover, we define the space V

$$V := \{v \in L^2(\Omega)^3 \, : \, \mathrm{div}\, v_{|\Omega_1} = 0 \text{ and } \mathrm{div}\, v_{|\Omega_2} = 0 \text{ and } \langle v_{|\Omega_2} \cdot \nu, 1\rangle_\Gamma = 0\}.$$

These spaces may be defined on the fields of real or complex numbers. Due to our application, the state function y is assumed to be real. In the weak formulations of our state equations, the test functions z are taken from the associated complex spaces.

For defining the notion of a weak solution of (2.3), we introduce the following sesquilinear form $a_0 : Y(\Omega) \times Y(\Omega) \to \mathbb{C}$:

$$a_0(y, z) = \int_\Omega \mu^{-1} \mathrm{curl}\, y \cdot \mathrm{curl}\, \bar{z}\, dx + e^{i\frac{\pi}{4}} \int_{\Omega_1} \mathrm{div}\, y_1 \, \mathrm{div}\, \bar{z}_1\, dx + e^{i\frac{\pi}{4}} \int_{\Omega_2} \mathrm{div}\, y_2 \, \mathrm{div}\, \bar{z}_2\, dx. \qquad (2.6)$$

In this definition, y_j stands for $y_{|\Omega_j}$, $j = 1, 2$, i denotes the imaginary unit and $\bar{z}$ the complex conjugate function of z. Since this is the only position, where the complex unit i appears, there should not be any confusion with the use of i for the electrical current.

DEFINITION 2.1. *A function $y : [0, T] \to Y(\Omega)$ is is said to be a weak solution of the system* (2.3), *if it enjoys the regularity properties $y \in L^2(0, T; Y(\Omega))$, $\sigma y \in C([0, T], V)$ and $\sigma y_t \in L^1(0, T; Y(\Omega)')$, and there holds*

$$
\begin{aligned}
\langle \sigma y_t(t), \, \bar{z}\rangle_{Y(\Omega)', Y(\Omega)} + a_0(y(\cdot, t), \bar{z}) &= i(t) \int_\Omega e(x) \cdot \bar{z}(x)\, dx \quad \forall z \in Y(\Omega), \text{ for a.a. } t \in (0, T), \\
y(x, 0) &= y_0(x) \quad \text{for a.a. } x \in \Omega_1.
\end{aligned}
$$
$$(2.7)$$

Here, we wrote for short $y_t := \partial y / \partial t$.

Moreover, we introduce the set of admissible controls

$$I_{ad} = \{i \in L^2(0, T) \, : \, \alpha \le i(t) \le \beta \text{ for a.a. } t \in (0, T)\}. \qquad (2.8)$$

We know from Corollary 3.12 in Nicaise and Tröltzsch [19] that, to each $i \in L^2(0, T)$, there exists a unique weak solution y of (2.3) provided that $y_0 \in H(\mathrm{div} = 0, \Omega_1)$. We denote this solution y by y_i, where the subscript indicates that y is associated to the control i. We do not indicate the dependence on y_0, since the initial data y_0 remain fixed. The mapping $i \mapsto y_i$ is continuous, cf. estimate (33) of Corollary 3.8 in [19] (to apply this Corollary, take $f(x, t) := e(x)\, i(t)$ there).

Now we are able to define our first optimal control problem:

$$\text{(OCP1)} \qquad \min_{i \in I_{ad}} J(y_i, i).$$

THEOREM 2.2. *The optimal control problem* (OCP1) *has a unique optimal control i^*.*

This result follows in a standard way by the weak compactness of the set I_{ad}, the continuity and affine-linearity of the mapping $i \mapsto y_i$, and by the weak lower semicontinuity of the *reduced objective function $\hat{J} : L^2(0, T) \to \mathbb{R}$,*

$$\hat{J} : i \mapsto J(y_i, i).$$

Let us denote for convenience the (optimal) state associated with i^* by $y^* := y_{i^*}$. In the next section, we derive the necessary optimality conditions for i^*.

6

2.2.2. Necessary optimality conditions. It is well known that i^* must satisfy the variational inequality

$$\hat{J}'(i^*)(i - i^*) \geq 0 \quad \forall i \in I_{ad}. \tag{2.9}$$

Expanding $\hat{J}'$, we obtain more explicitely

$$\lambda_T \int_{\Omega_1} (y_{i^*}(\cdot, T) - y_T(\cdot)) \cdot (y_i(\cdot, T) - y_{i^*}(\cdot, T))\, dx + \lambda_Q \int_{Q_1} (y_{i^*} - y_Q) \cdot (y_i - y_{i^*})\, dxdt$$
$$+\lambda_i \int_0^T i^* \, (i - i^*)\, dt \geq 0 \quad \forall i \in I_{ad}. \tag{2.10}$$

By an adjoint state, the state function y can be eliminated from the inequality above in a standard way. To this aim, we introduce the following adjoint equation:

$$\begin{cases}
-\sigma_0 \dfrac{\partial p}{\partial t}(x, t) + \operatorname{curl} \mu^{-1} \operatorname{curl} p(x, t) &=& \lambda_Q(y^*(x, t) - y_Q(x, t)) & \text{in} & \Omega_1 \times (0, T) \\
\operatorname{curl} \mu^{-1} \operatorname{curl} p(x, t) &=& 0 & \text{in} & \Omega_2 \times (0, T) \\
p(x, t) \times \nu &=& 0 & \text{on} & \partial\Omega \times (0, T) \\
\sigma_0 \, p(x, T) &=& \lambda_T(y^*(x, T) - y_T(x)) & \text{in} & \Omega_1.
\end{cases} \tag{2.11}$$

LEMMA 2.3. *Suppose that $y_Q \in L^2(0, T; L^2(\Omega_1)^3)$ satisfies $\operatorname{div} y_Q(\cdot, t) = 0$ for a.a. $t \in (0, T)$ and that also $\operatorname{div} y_T = 0$ is fulfilled. Then there exists a unique solution p^* of the adjoint equation (2.11); p^* enjoys the regularity $p^* \in L^2(0, T; Y(\Omega))$, $\sigma p_t^* \in L^1(0, T; Y(\Omega)')$, and $p^*_{|\Omega_1} \in C([0, T], H(\operatorname{div} = 0, \Omega_1))$.*

Proof. The result is obtained by the transformation of time $\tau = T - t$. In this way, the adjoint equation is transformed to a forward parabolic-elliptic equation for the new function $\tilde{p}(x, \tau) = p(x, T - t)$.

To apply Corollary 3.12 of [19], we need that the associated right-hand side (in [19] denoted by f) and the initial data satisfy the assumptions $f \in L^2(0, T; Y(\Omega)')$, $\operatorname{div} f = 0$ in Q_1, and that $\operatorname{div} y_0 = 0$ in Ω_1. In our adjoint equation, this amounts to the requirements $y - y_Q \in L^2(0, T; Y(\Omega)')$, $\operatorname{div}(y - y_Q) = 0$ in Q_1, and $\operatorname{div}(y(T) - y_T) = 0$ in Ω_1. Obviously, this is ensured by our assumptions on y_T and y_Q and by the regularity of y^*. ☐

We use p^* for eliminating the state functions in the variational inequality (2.10).

LEMMA 2.4. *Let y^* be the solution associated with an arbitrary (not necessarily optimal) $i^* \in L^2(0, T)$ and take $i \in L^2(0, T)$ with associated state y_i. Assume that y_Q and y_T satisfy the assumptions stated in Lemma 2.3. Define the adjoint state p^* as the unique solution to the adjoint equation (2.11). Then there holds*

$$\lambda_T \int_{\Omega_1} (y^*(x, T) - y_T(x)) \cdot (y_i(x, T) - y^*(x, T))\, dx + \lambda_Q \int_{Q_1} (y^* - y_Q) \cdot (y_i - y^*)\, dxdt$$
$$= \int_0^T \left(\int_{\Omega_1} e(x) \cdot p^*(x, t)\, dx \right) (i - i^*)\, dt. \tag{2.12}$$

Proof. We introduce the function $y := y_i - y^* = y_{i - i^*}$; then it holds $y(0)|_{\Omega_1} = 0$. Since y_t and p_t^* only belong to $L^1(0, T; V')$, we proceed by a density argument: $H^1(0, T)$ is dense in $L^2(0, T)$, hence

7

we can select a sequence $(i_n)_n$ in $H^1(0,T)$ such that $i_n \to (i - i^*)$ in $L^2(0,T)$ as $n \to \infty$. Let y_n denote the solution of (2.3) associated with $i := i_n$ and $y_0 = 0$. We have $y_n \to y$ in $L^2(0,T;L^2(\Omega)^3)$ and $y_{n|\Omega_1} \to y_{|\Omega_1}$ in $C([0,T],L^2(\Omega_1)^3)$.

Now we follow the arguments of the proof of Thm. 3.14 in [19]. We formally differentiate the state equation (2.3) with respect to t. The right-hand side $e\,i_n'$ belongs to $L^2(0,T;H(\mathrm{div} = 0,\Omega))$, hence the differentiated equation has a solution $w_n \in L^2(0,T,V)$ with $w_{n|\Omega_1} \in C([0,T],L^2(\Omega_1)^3)$. The functions

$$y_n(t) = \int_0^t w_n(s)\,ds$$

are solutions of (2.3) with i_n instead of i and satisfy $(y_n)_{t|\Omega_1} \in C([0,T],L^2(\Omega_1)^3)$, cf. formula (55) in [19]. Notice also that the initial value of y_n is zero, hence smooth and divergence free.

In view of this, we also have $(\sigma\,y_n)_t \in C([0,T],L^2(\Omega)^3) \subset C([0,T],Y(\Omega)')$. Now, we multiply the adjoint equation by the function y_n and integrate over Q to obtain

$$-\int_0^T \int_\Omega \sigma\,p_t^* \cdot y_n\,dxdt + \int_0^T a_0(p^*(t), y_n(t))\,dt = \int_0^T \int_{\Omega_1} \lambda_Q\,(y^* - y_Q) \cdot y_n\,dxdt.$$

Notice that all y_n and also p^* are real functions, hence $y_n = \bar{y}_n$ and $p^* = \bar{p}^*$ so that it does not matter on which side of the sesquilinear forms the functions stand.

In the equation above, we have written for convenience

$$\langle \sigma p_t^*,\, y_n \rangle_{Y(\Omega)',Y(\Omega)} =: \int_0^T \int_\Omega \sigma\,p_t^* \cdot y_n\,dxdt$$

although the integrals are possibly not well defined. We shall apply this notation also later, since this supports the understanding of integration by parts.

Integrating by parts in the first integral, it follows

$$\int_0^T \int_\Omega \sigma\,p^* \cdot (y_n)_t\,dxdt + \int_0^T a_0(p^*(t), y_n(t))\,dt$$
$$= \int_{\Omega_1} \sigma_0\,p^*(x,T) \cdot y_n(x,T)\,dx + \int_0^T \int_{\Omega_1} \lambda_Q\,(y^* - y_Q) \cdot y_n\,dxdt$$
$$= \int_{\Omega_1} \lambda_T\,(y^*(x,T) - y_T(x)) \cdot y_n(x,T)\,dx + \int_0^T \int_{\Omega_1} \lambda_Q\,(y^* - y_Q) \cdot y_n\,dxdt,$$

where we have finally inserted the given terminal condition for $p^*(T)$. On the other hand, multiplying the equation for y_n by p^*, we find

$$\int_0^T \int_\Omega \sigma\,(y_n)_t \cdot p^*\,dxdt + \int_0^T a_0(y_n^*(t), p^*(t))\,dt = \int_0^T \left(\int_{\Omega_1} e(x) \cdot p^*(x,t)\,dx \right) i_n(t)\,dt.$$

Obviously, the left-hand sides of the last two equations are equal, hence the same holds for their right-hand sides,

$$\int_{\Omega_1} \lambda_T\,(y^*(x,T) - y_T(x)) \cdot y_n(x,T)\,dx + \lambda_Q \int_{Q_1} (y^* - y_Q) \cdot y_n\,dxdt = \int_0^T \left(\int_{\Omega_1} e \cdot p^*\,dx \right) i_n\,dxdt.$$

8

Passing to the limit $n \to \infty$, we arrive at the desired equation (2.12). □

Now the necessary optimality condition for i^* is an immediate consequence.

THEOREM 2.5. *Let i^* be the optimal control of problem* (OCP1), $y^* = y_{i^*}$ *be the associated (optimal) state. Assume that $\operatorname{div} y_Q(\cdot, t) = 0$ for a.a. $t \in (0, T)$ and that $\operatorname{div} y_T = 0$ holds. Let the adjoint state p^* be the solution to* (2.11). *Then i^* must satisfy the variational inequality*

$$\int_0^T \left(\int_{\Omega_1} e(x) \cdot p^*(x, t)\, dx + \lambda_i\, i^*(t) \right) \left(i(t) - i^*(t) \right) dt \geq 0 \quad \forall i \in I_{ad}. \tag{2.13}$$

The theorem follows immediately from (2.10) and Lemma 2.4, equation (2.12). If $\lambda_i > 0$, then, by a standard pointwise discussion of (2.13), we arrive at the projection formula

$$i^*(t) = \mathbb{P}_{[\alpha, \beta]} \left(-\frac{1}{\lambda_i} \int_{\Omega_1} e(x) \cdot p^*(x, t)\, dx \right) \quad \text{for a.a. } t \in (0, T). \tag{2.14}$$

Here, $\mathbb{P}_{[\alpha, \beta]} : \mathbb{R} \to \mathbb{R}$ is defined by $\mathbb{P}_{[\alpha, \beta]}(v) = \max(\alpha, \min(\beta, v))$. We apply this formula for testing the precision of numerically computed optimal controls.

Moreover, the reduced gradient $\nabla \hat{J}(i^*)$, i.e. the Hilbert space representation of the derivative $\hat{J}'(i^*)$ at an arbitrary not necessarily optimal i^*, is given by

$$(\nabla \hat{J}(i^*))(t) = \int_{\Omega_1} e(x) \cdot p^*(x, t)\, dx + \lambda_i\, i^*(t), \quad t \in [0, T]. \tag{2.15}$$

This is the basis for implementing gradient type methods.

2.3. Controlled electrical voltage.

2.3.1. An integro-differential model. We have already pointed out that controlling the electrical current is not realistic in practice, because only the voltage can be chosen more or less arbitrarily. Therefore, we now consider the electrical voltage u as control function.

One might think that, for given u, the electrical current i is just obtained by Ohm's law, i.e. $i = u/R_c$, where R_c is the resistance of the coil windings. However, any current i in the coil generates a magnetic field – the field we want to influence – and generating this field counteracts the electrical current. Therefore, we have to consider also the induction law. This eventually leads to the following integro-differential equation as a substitute for Ohm's law:

$$\begin{aligned} \int_\Omega \frac{\partial y}{\partial t}(x, t) \cdot e(x)\, dx + R_c\, i(t) &= u(t), \quad t \in (0, T), \\ i(0) &= i_0. \end{aligned} \tag{2.16}$$

Since e vanishes outside the coil Ω_c, the integral above is one on Ω_c. Moreover, now we regard Ω_c as part of the nonconducting domain (this is a consequence of the modeling), hence $\Omega_c \subset \Omega_2$ holds here. The integro-differential equation (2.16) is derived in our paper [18], where also the practical background of time-optimal control in flow measurement devices is sketched.

Let us explain for convenience of the reader the derivation of the formula (2.16). We follow our arguments of [18]: Thanks to the induction law, it must hold

$$\frac{d}{dt}\Psi(t) + R_c\, i(t) = u(t),$$

9

where

$$\Psi(t) = \int_{\mathcal{F}_c} B(t) \cdot dS$$

is the total magnetic flux through the area spanned by all windings and $\mathcal{F}_c$ is the surface spanned by the windings of the coil. Now, we argue as follows: If the coil consists of only one winding, the surface $\mathcal{F}_c$ is bounded by the closed curve $\partial \mathcal{F}_c$ of this winding. We obtain

$$\frac{d}{dt}\Psi(t) = \int_{\mathcal{F}_c} \frac{\partial B}{\partial t}(t) \cdot dS = \int_{\mathcal{F}_c} \frac{\partial}{\partial t}(\operatorname{curl} y(t)) \cdot dS = \int_{\mathcal{F}_c} \operatorname{curl} \frac{\partial y}{\partial t}(t) \cdot dS = \oint_{\partial \mathcal{F}_c} \frac{\partial y}{\partial t}(t) \cdot ds,$$

where the last equation follows from the theorem of Stokes. If the coil has N_c windings, then we have to consider the union of the surfaces $\mathcal{F}_{w_i}$ spanned by all windings w_i,

$$\mathcal{F}_c = \bigcup_{i=1}^{N_c} \mathcal{F}_{w_i}.$$

We obtain

$$\frac{d}{dt}\Psi(t) = \sum_{i=1}^{N_c} \oint_{\partial \mathcal{F}_{w_i}} \frac{\partial y}{\partial t}(t) \cdot ds \approx \frac{N_c}{|\omega_c|} \int_{\Omega_c} \frac{\partial y}{\partial t}(t) \cdot w \ dx = \int_{\Omega_c} \frac{\partial y}{\partial t}(t) \cdot e \ dx.$$

Here, we used the current direction $w = e/|e|$ with $\operatorname{div} w = 0$ and $|w| = 1$.

Complementing the original system by this equation, we arrive at the integro-differential model

$$\begin{cases}
\sigma_0 \dfrac{\partial y}{\partial t}(x,t) + \operatorname{curl} \mu^{-1} \operatorname{curl} y(x,t) &=& 0 & \text{in} & \Omega_1 \times (0,T) \\
\operatorname{curl} \mu^{-1} \operatorname{curl} y(x,t) &=& e(x)\,i(t) & \text{in} & \Omega_2 \times (0,T) \\
y(x,t) \times \nu &=& 0 & \text{on} & \partial\Omega \times (0,T) \\
y(x,0) &=& y_0(x) & \text{in} & \Omega_1, \\[2mm]
\displaystyle\int_\Omega \dfrac{\partial y}{\partial t}(x,t) \cdot e(x) \, dx + R_c\, i(t) &=& u(t) & \text{in} & (0,T) \\
i(0) &=& i_0.
\end{cases} \qquad (2.17)$$

In this setting, the definition of the sets Ω_j, $j = 1, 2$, differs from that in (2.3). Now, they are defined by

$$\Omega_1 = \Omega_{tb}, \qquad \Omega_2 = \Omega \setminus \bar{\Omega}_{tb}.$$

The analysis of (2.17) is more delicate than that for (2.3). In a first step, we eliminate the current i by the integro-differential part of (2.17),

$$i(t) = R_c^{-1}\left(u(t) - \int_\Omega \frac{\partial y}{\partial t}(x,t) \cdot e(x)\, dx\right) \qquad (2.18)$$

and insert this in the differential part. We get the degenerate parabolic integro-differential equation

$$
\begin{cases}
\sigma_0 \dfrac{\partial y}{\partial t}(x,t) + \operatorname{curl} \mu^{-1} \operatorname{curl} y(x,t) &= 0 & \text{in} \quad \Omega_1 \times (0,T) \\
R_c^{-1} \displaystyle\int_{\Omega_1} \dfrac{\partial y}{\partial t}(\xi,t) \cdot e(\xi)\, d\xi\, e(x) + \operatorname{curl} \mu^{-1} \operatorname{curl} y(x,t) &= R_c^{-1}\, e(x)\, u(t) & \text{in} \quad \Omega_2 \times (0,T) \\
y(x,t) \times \nu &= 0 & \text{on} \quad \partial\Omega \times (0,T) \\
y(x,0) &= y_0(x) & \text{in} \quad \Omega_1.
\end{cases}
\tag{2.19}
$$

By this substitution, we have lost the initial condition $i(0) = i_0$. Moreover, it is not obvious that i must be continuous so that $i(0)$ is well defined. Therefore, we follow a detour. First we complete the system (2.19) by the somehow artificial initial condition

$$
\int_{\Omega_1} y(x,0) \cdot e(x)\, dx = \alpha_0
\tag{2.20}
$$

with some given real number α_0. We consider an associated optimal control problem for u and show that this is solvable. Next, as a conclusion of the optimality conditions, we deduce that the optimal voltage u^* belongs to $H^1(0,T)$. Finally, Theorem 2.10 yields $i^* \in H^1(0,T)$ so that i^* is continuous.

We are able to fix α_0 in such a way that the initial condition $i(0) = i_0$ is satisfied. This closes the loop so that we can later return to the original model (2.17).

2.3.2. Optimal control problem and auxiliary control problem. In what follows, we write for convenience $U_{ad} := I_{ad}$ although the set of admissible controls remains (mathematically) unchanged, i.e. it is given by upper and lower bounds α, β. The full optimal control problem "optimal voltage" that also includes the electrical current i as part of the state functions is

$$
\text{(OCP2)} \qquad\qquad \min_{u \in U_{ad}}\ J(y_u, u),
$$

where J has the same principal form as in (2.5),

$$
J(y,u) := \frac{\lambda_T}{2} \int_{\Omega_1} |y(x,T) - y_T(x)|^2\, dx + \frac{\lambda_Q}{2} \iint_{Q_1} |y(x,t) - y_Q(x,t)|^2\, dx dt + \frac{\lambda_u}{2} \int_0^T u^2(t)\, dt, \tag{2.21}
$$

but for convenience we denote the regularization parameter associated with the control by $\lambda_u \geq 0$. Here, y_u denotes the solution of (2.17) that is associated with the control u.

At this point, the definition of y_u this is formal, since we do not know if the underlying system (2.17) admits a continuous electrical current i as part of the solution. Therefore, the initial condition for i is possibly not well posed. In view of this, we first discuss the auxiliary control problem

$$
\text{(OCP2}_{\text{aux}}) \qquad\qquad \min_{u \in U_{ad}}\ J(y_u, u),
$$

where y_u is the solution to the simplified state equation (2.19) subject to the initial condition (2.20).

For defining a weak solution to the system (2.19) we have to add to a_0 a term accounting for the integrodifferential part of (2.19), cf. Definition 2.1.

11

DEFINITION 2.6. *A function $y : [0, T] \to Y(\Omega)$ is said to be a weak solution of the system (2.19), if y has the regularity properties formulated in Definition 2.1, fulfills that $t \mapsto \int_{\Omega_2} e(x) \cdot y(x, t) \, dx$ belongs to $H^1(0, T)$, and satisfies the equations*

$$\langle \sigma y_t(t) \,, \, \bar{z} \rangle_{Y(\Omega)', Y(\Omega)} + a_0(y(\cdot, t), \bar{z}) + R_c^{-1} \left(\int_{\Omega_2} e(x) \cdot y_t(x, t) \, dx \right) \left(\int_{\Omega_2} e(x) \cdot \bar{z}(x) \, dx \right)$$
$$= R_c^{-1} \int_{\Omega_2} e(x) \cdot \bar{z}(x) \, dx \, u(t) \quad \forall z \in Y(\Omega), \text{ for a.a. } t \in (0, T), \tag{2.22}$$

$$y(x, 0) = y_0(x) \quad \text{for a.a. } x \in \Omega_1, \tag{2.23}$$

$$\int_{\Omega_2} y(x, 0) \cdot e(x) \, dx = \alpha_0. \tag{2.24}$$

The following result follows from Corollary 3.13 in [19]:

LEMMA 2.7. *For all given $u \in L^2(0, T)$, divergence free $y_0 \in L^2(\Omega_1)^3$, and $\alpha_0 \in \mathbb{R}$, the system (2.19), (2.20) has a unique weak solution $y \in L^2(0, T; Y(\Omega))$ with the following regularity properties: There is a constant $c > 0$ not depending on f and y_0 such that*

$$\|y\|_{L^2(0, T; Y(\Omega))} + \|\sigma y_t\|_{L^1(0, T; Y(\Omega)')}$$
$$+ \left\| \int_{\Omega_2} y(x, \cdot) \cdot e(x) \, dx \right\|_{H^1(0, T)} \leq c \left(|\alpha_0| + \|u\|_{L^2(0, T)} + \|y_0\|_V \right). \tag{2.25}$$

By this Lemma, we easily deduce again that the optimal control problem $(\text{OCP2}_{\text{aux}})$ has a unique optimal control u^* with associated optimal state $y^* := y_{u^*}$.

2.4. Necessary optimality conditions for $(\text{OCP2}_{\text{aux}})$**.** To establish the associated necessary optimality conditions, we begin as in the preceding section. Completely analogous to (2.10), u^* and y^* must obey the variational inequality

$$\lambda_T \int_{\Omega_1} (y^*(\cdot, T) - y_T(\cdot)) \cdot (y_u(\cdot, T) - y_{u^*}(\cdot, T)) \, dx + \lambda_Q \int_{Q_1} (y^* - y_Q) \cdot (y_u - y_{u^*}) \, dxdt$$
$$+ \lambda_u \int_0^T u^* (u - u^*) \, dt \geq 0 \quad \forall u \in U_{ad}. \tag{2.26}$$

To reduce this inequality to one for u only, we define the following adjoint equation:

$$\begin{cases} -\sigma_0 \dfrac{\partial p}{\partial t}(x, t) + \operatorname{curl} \mu^{-1} \operatorname{curl} p(x, t) &= \lambda_Q \left(y^*(x, t) - y_Q(x, t) \right) & \text{in} \quad Q_1 \\[2mm] -R_c^{-1} \displaystyle\int_{\Omega_2} \dfrac{\partial p}{\partial t}(\xi, t) \cdot e(\xi) \, d\xi \, e(x) + \operatorname{curl} \mu^{-1} \operatorname{curl} p(x, t) &= 0 & \text{in} \quad Q_2 \\[2mm] p(x, t) \times \nu &= 0 & \text{on} \quad \Sigma_T \\[2mm] \sigma_0 \, p(x, T) &= \lambda_T \left(y^*(x, T) - y_T(x) \right) & \text{in} \quad \Omega_1 \\[2mm] \displaystyle\int_{\Omega_2} p(x, T) \cdot e(x) \, dx &= 0. \end{cases} \tag{2.27}$$

12

THEOREM 2.8. *Assume that u^* is the optimal control of* (OCP2$_{\mathrm{aux}}$) *and y^* is the associated state. Let the conditions $\mathrm{div}\, y_Q(\cdot, t) = 0$ for a.a. $t \in (0, T)$ and $\mathrm{div}\, y_T = 0$ be satisfied.*

Then there exists an associated unique weak solution p^* of (2.27) *having the same regularity properties as y^* such that*

$$\int_0^T \left(\int_{\Omega_2} e(x) \cdot p^*(x, t)\, dx + \lambda_u\, u^*(t) \right) \left(u(t) - u^*(t) \right) dt \geq 0 \quad \forall u \in U_{ad}. \tag{2.28}$$

Proof. We have to consider the difference $y := y_u - y_{u^*} = y_{u-u^*}$. Let us assume that $v := u - u^*$ belongs to $H^1(0, T)$. If not, we can apply a density argument as in the proof of Lemma 2.4 and consider a sequence of functions $v_n \in H^1(0, T)$ converging to v in $L^2(0, T)$.

Notice again that y and p^* are functions with real-valued components. Now, we use the adjoint state as test function in the weak formulation of the state equation (2.19) and obtain after adding the two parts

$$\int_0^T \int_\Omega \sigma \frac{\partial y}{\partial t} \cdot p^*\, dxdt + R_c^{-1} \int_0^T \int_\Omega \int_{\Omega_2} \frac{\partial y}{\partial t}(\xi, t) \cdot e(\xi)\, d\xi\, e(x) \cdot p^*(x, t)\, dxdt$$
$$+ \int_0^T a_0(y(t), p^*(t))\, dt = R_c^{-1} \int_{Q_2} e(x) \cdot p^*(x, t)\, v(t)\, dxdt. \tag{2.29}$$

Due to our working assumption on v, the derivative $\partial y/\partial t$ is sufficiently smooth so that the first integral in the equation above is well defined. Analogously, we use the state difference y as test function in the adjoint equation (2.27) and obtain

$$-\int_0^T \int_\Omega \sigma \frac{\partial p^*}{\partial t} \cdot y\, dxdt - R_c^{-1} \int_0^T \int_{\Omega_2} \int_{\Omega_2} \frac{\partial p^*}{\partial t}(\xi, t) \cdot e(\xi)\, d\xi\, e(x) \cdot y(x, t)\, dxdt$$
$$+ \int_0^T a_0(y(t), p^*(t))\, dt = \int_0^T \int_{\Omega_1} \lambda_Q \left(y^*(x, t) - y_Q(x, t) \right) \cdot y(x, t)\, dxdt.$$

In the integrals containing $\partial p^*/\partial t$, we perform an integration by parts and find

$$-\int_{\Omega_1} \lambda_T \left(y^*(x, T) - y_T(x) \right) \cdot y(x, T)\, dx + \int_0^T \int_\Omega \sigma \frac{\partial y}{\partial t} \cdot p^*\, dxdt$$
$$+ \int_0^T a_0(y(t), p^*(t))\, dt - R_c^{-1} \int_{\Omega_2} p^*(\xi, T) \cdot e(\xi)\, d\xi \int_{\Omega_2} y(x, T) \cdot e(x)\, dx$$
$$+ R_c^{-1} \int_0^T \int_{\Omega_2} \int_{\Omega_2} \frac{\partial y}{\partial t}(\xi, t) \cdot e(\xi)\, d\xi\, e(x) \cdot p^*(x, t)\, dxdt \tag{2.30}$$
$$= \int_0^T \int_{\Omega_1} \lambda_Q \left(y^*(x, t) - y_Q(x, t) \right) \cdot y(x, t)\, dxdt,$$

where we have used that $y(x, 0) = 0$ and that $\sigma_0 p^*(x, T) = \lambda_T \left(y^*(x, T) - y_T(x) \right)$. In view of

$$\int_{\Omega_2} p^*(x, T) \cdot e(x)\, dx = 0,$$

13

subtracting the equation (2.30) from (2.29), we deduce

$$\int_{\Omega_1} \lambda_T \left(y^*(x,T) - y_T(x)\right) \cdot y(x,T)\,dx + \int_0^T \int_{\Omega_1} \lambda_Q \left(y^*(x,t) - y_Q(x,t)\right) \cdot y(x,t)\,dxdt$$
$$= \int_{Q_2} e(x) \cdot p^*(x,t)\,v(t)\,dxdt = \int_0^T \int_{\Omega_2} e(x) \cdot p^*(x,t)\,(u(t) - u^*(t))\,dxdt.$$

Inserting the right-hand side of this equation in the variational inequality (2.26), we immediately verify the desired inequality (2.28). $\qquad\square$

For $\lambda_u > 0$, a pointwise discussion of the variational inequality (2.28), yields the projection formula

$$u^*(t) = \mathbb{P}_{[\alpha,\beta]} \left(-\frac{1}{\lambda_u} \int_{\Omega_2} e(x) \cdot p^*(x,t)\,dx \right) \qquad \text{for a.a. } t \in (0,T). \tag{2.31}$$

COROLLARY 2.9. *Under the assumptions of Theorem 2.8, the optimal control u^* for* (OCP2$_{\mathrm{aux}}$) *belongs to $H^1(0,T)$.*

Proof. The adjoint state p^* enjoys the regularity of y^* stated in Lemma 2.7, hence the function

$$q^* : t \mapsto \int_{\Omega_2} e(x) \cdot p^*(x,t)\,dx$$

belongs to $H^1(0,T)$. The same holds for the function $t \mapsto \mathbb{P}_{[\alpha,\beta]}(q^*(t))$, because $f \in H^1(0,T)$ implies that also $\max(f(\cdot),\alpha)$ and $\min(f(\cdot),\beta)$ belong to $H^1(0,T)$, cf. Kinderlehrer and Stampacchia [12]. Therefore, also the optimal control

$$u^* = \mathbb{P}_{[\alpha,\beta]}(q(\cdot)^*) = \min\left(\max\left(\alpha, q(\cdot)^*\right), \beta\right)$$

belongs to $H^1(0,T)$. $\qquad\square$

The reduced gradient is now given by

$$(\hat{J}'(u^*))(t) = \int_{\Omega_2} e(x) \cdot p^*(x,t)\,dx + \lambda_u\,u^*(t), \quad t \in [0,T]. \tag{2.32}$$

2.4.1. Necessary optimality conditions for (OCP2). By Corollary 2.9 we know that the optimal control u^* of (OCP2$_{\mathrm{aux}}$) belongs to $H^1(0,T)$. This implies that also the associated optimal electrical current i^* enjoys this regularity. To see this, we recall the following results of [19]:

THEOREM 2.10. *Assume in addition to the assumptions stated in Lemma 2.7 that it holds $\mathrm{curl}\,\mu^{-1}\mathrm{curl}\,y_0 \in L^2(\Omega_1)^3$, $e \neq 0$, and $u \in H^1(0,T)$. Then the solution y of (2.19) belongs to $H^1(0,T;H(\mathrm{curl},\Omega))$. Moreover, then the function i is continuous on $[0,T]$.*

Proof. Thanks to the assumptions of Lemma 2.7, $\mathrm{curl}\,\mu^{-1}\mathrm{curl}\,y_0 \in L^2(\Omega_1)^3$, $u \in H^1(0,T)$, and the property $e \neq 0$, we can apply Theorem 3.14 of [19] to get $y \in H^1(0,T;H(\mathrm{curl},\Omega))$. Clearly, this implies the claimed regularity of y. Next, we invoke Lemma 3.15 of [19] that ensures $i \in H^1(0,T)$ provided that $y|_{\Omega_2}$ belongs to $C([0,T],H(\mathrm{curl}\,(\Omega_2))$. This is granted by $y \in H^1(0,T;H(\mathrm{curl},\Omega))$.
$\qquad\square$

In view of these results, the optimal state i^* is continuous on $[0,T]$ and the initial value $i^*(0)$ is well defined. Therefore, we are justified to return to the original full state equations (2.17) for the pair of states (y,i).

14

Let us now fix the notion of a weak solution (y, i) for the full system (2.17).

DEFINITION 2.11. *Given* $u \in H^1(0, T)$, $i_0 \in \mathbb{R}$ *and* $y_0 \in L^2(\Omega_1)^3$ *with* $curl(\mu^{-1} curl\, y_0) \in$ $L^2(\Omega_1)^3$, *we say that* (y, i) *is a weak solution of* (2.17), *if* $y \in H^1(0, T; H(curl, \Omega))$ *obeys the regularity stated in Lemma 2.7, i belongs to $C[0, T]$, the conditions $y(\cdot, 0) = y_0$ and $i(0) = i_0$ are satisfied, the fifth identity of* (2.17) *is fulfilled for a.a.* $t \in (0, T)$ *and*

$$\langle \sigma y_t(\cdot, t); \bar{z} \rangle_{Y(\Omega)', Y(\Omega)} + a_0(y(\cdot, t), \bar{z}) = i(t) \int_\Omega e(x) \cdot \bar{z}(x)\, dx \quad \forall z \in Y(\Omega),\ \textit{for a.a.}\ t \in (0, T). \quad (2.33)$$

By Theorem 2.10 and the known H^1-regularity of the optimal control u^*, the original state system (2.17) has a unique weak solution (y^*, i^*). This information justifies to consider the full system. In the analysis, we can use it to set up the necessary optimality conditions for u^*. For the numerical treatment, we also consider this full system, because after a finite element discretization with respect to the space, the associated system of integro-differential equations is uniquely solvable for all $u \in L^2(0, T)$.

2.4.2. Optimality system for problem (OCP2). In view of the higher regularity of u^*, we obtain the following result on optimality conditions for the control problem (OCP2):

THEOREM 2.12. *Assume that* $curl(\mu^{-1} curl\, y_0) \in L^2(\Omega_1)^3$ *and let* u^* *be the optimal control of problem* (OCP2$_{\text{aux}}$). *Then there exist a unique pair* (p^*, q^*) *of adjoint states satisfying the (full) adjoint system*

$$
\begin{cases}
-\sigma_0 \dfrac{\partial p}{\partial t}(x, t) + curl\,\mu^{-1}\, curl\, p(x, t) &=& \lambda_Q(y^*(x, t) - y_Q(x, t)) & in & Q_1 \\[2mm]
-\dfrac{1}{R_c} \dfrac{dq}{dt}(t)\, e(x) + curl\,\mu^{-1}\, curl\, p(x, t) &=& 0 & in & Q_2 \\[2mm]
p(x, t) \times \nu &=& 0 & on & \Sigma_T \\[2mm]
q(t) &=& \displaystyle\int_{\Omega_2} p(x, t) \cdot e(x)\, dx & in & (0, T) \\[2mm]
\sigma_0\, p(x, T) &=& \lambda_T\,(y^*(x, T) - y_T(x)) & in & \Omega_1 \\[2mm]
q(T) &=& 0
\end{cases}
\quad (2.34)
$$

such that the variational inequality

$$\int_0^T \left(q^*(t) + \lambda_u\, u^*(t)\right) \left(u(t) - u^*(t)\right) dt \geq 0 \quad \forall u \in U_{ad} \quad (2.35)$$

is satisfied.

Proof. The result follows immediately from Theorem 2.8 by substituting

$$q^*(t) := \int_{\Omega_2} p^*(x, t) \cdot e(x)\, dx.$$

□

The function q^* can be viewed as the Lagrange multiplier associated with the integro-differential equation

$$\int_{\Omega_2} \frac{\partial y}{\partial t}(x, t) \cdot e(x)\, dx + R_c\, i(t) = u(t).$$

This can be easily verified by applying a formal Lagrange technique for deriving the optimality system.

Numerically, it is easier to handle the full system including the electrical current i than to work with the simplified system, where the current is eliminated. In particular, the initial condition $i(0) = i_0$ is easier to handle than the auxiliary initial condition $\int_{\Omega_2} y(x,0) \cdot e(x) \, dx = \alpha_0$, where α_0 has to be chosen in the right way so that the initial condition for i is fulfilled, cf. [19].

REMARK 3. *We know by Corollary 2.9 that the optimal control u^* of* (OCP2$_{\text{aux}}$) *or* (OCP2) *belongs to $H^1(0,T)$ provided that the assumptions of Theorem 2.8 are satisfied. Therefore, u^* is also the solution to the problem*

$$\min_{u \in U_{ad} \cap H^1(0,T)} \quad J(y_u, u)$$

and the variational inequalities (2.28) *(or equivalently* (2.35)*) are satisfied with $U_{ad} \cap H^1(0,T)$ substituted for U_{ad}.*

Numerically it might be helpful to implement such smoother control functions, for instance by a piecewise linear approximation of u. Notice, however, that a projection formula such as (2.31) *does not hold for piecewise linear approximations of u while it is true for an approximation by step functions.*

3. Numerical Examples.

3.1. Introduction. Solving the parabolic-elliptic evolution Maxwell equations numerically, we implemented a finite element method with respect to the space variable and the implicit Euler method with fixed step size in the time. For the following reasons, this generates very large scale linear algebraic equations:

First of all, the equations have to be solved in a 3D spatial domain. For the tube with coil, the problem can be transformed by cylindrical coordinates to one of dimension 2. We decided to avoid this simplification, because the geometry of the real application is more complicated and does not allow cylindrical coordinates (cf. the setting of an industrial DN50 sensor presented in Fig. 3.4). In Section 3.3, we briefly report on a real application to flow measurement. Second, switching in and off the electrical current leads to steep curves right after the initial time. Therefore, we had to apply very small time steps in the implicit Euler method so that a large number of linear algebraic equations had to be solved.

From the optimization point of view, large scale convex optimization problems with box constraints on the control function must be solved. This somehow dictated the choice of the numerical optimization method. Though the discretized optimal control problem is nothing more than a problem of quadratic optimization, available commercial solvers of quadratic programming will not be able to process a problem of that size at once. In view of this, we applied a standard projected gradient method and also the projected conjugate gradient method with exact step size. We approximated the reduced gradient of J by the solution of the discretized adjoint equation. This approach worked well for our academic geometries. However, the application to real sensors for flow measurement would require computation times in the range of months to achieve the needed precision, cf. Section 3.3. Therefore we invoked model order reduction by standard proper orthogonal decomposition (POD) with big success, cf. our presentation below.

We omit the details of all implementations, because we do not understand our paper as a contribution to the efficient numerical solution of the problems under consideration. We just want

to give the reader an impression on the numerical treatment of the problem and refer to [18], where we report more detailed on our computational experience.

All computations with academic geometries were done for a tube with coil of the following size:

Test geometry "tube with coil". *In our numerical tests with simplified geometry, the holdall domain Ω is a cube of side length $0.2\,m$ centered at the origin. The tube is taken parallel to one of the sides, centered in the cube. For the tube, we selected the following data:*

$$r_1 = 0.01\,m, \quad r_2 = 0.015\,m, \quad z_1 = -0.05\,m, \quad z_2 = 0.05\,m,$$

and

$$r_3 = 0.02\,m, \quad c_1 = -0.02\,m, \quad c_2 = 0.02\,m.$$

In the numerical examples, we concentrate on the optimal control of the electrical voltage u. Only this case is realistic for a practicable application. If the electrical current i is taken as control, then the application of the optimal solution in a sensor would need big jumps between different values of the current, which cannot be generated in an electrical circuit.

Moreover, the numerical treatment of the controlled voltage is more challenging than that for the controlled circuit. Readers who are interested in numerical results for the electrical current as control are referred to the PhD thesis [2].

We applied a conjugate gradient method for the numerical solution of the optimal control problem. For the convenience of the reader, we mention how the descent direction in the projected gradient method is determined. Let u_k be the current iterate and (y_k, i_k) be the associated state vector function. Then, in view of (2.32), we compute the reduced gradient by

$$g_k(t) := \int_{\Omega_2} e(x) \cdot p_k(x, t)\, dx + \lambda_u\, u_k(t),$$

where p_k is the adjoint state obtained as solution to (2.34) with y^* substituted by y_k, cf. also the equation defining q in (2.32). Then

$$\delta_k := -g_k$$

is a direction of descent provided that $g_k \neq 0$. However, the new iterate $u_k + s\,\delta_k$ might exceed the given box constraints for any step size $s > 0$. Therefore, a standard projection step must be included; we omit the further details.

3.2. Example 1: Optimal control for the geometry "tube with coil". We consider the optimal control problem (OCP2) with the equation (2.17) as state equation, where y_0 is given as the initial state for the vector potential y. The aim of the optimization is to reach $-y_0$ in short time.

Data for the Example. *We consider the geometry "tube with coil" for the following data:*
- *PDE data:*

$$\mu = 400, \quad \sigma = 10^6\,S/m, \quad R_c = 10\,\Omega, \quad N = 1600, \quad |\omega_c| = 0.005 \cdot 0.040 m^2, \quad T = 0.5\,s.$$

- *Weights and bounds:* We set $\lambda_T = 0$, $\lambda_Q = 10^5$, test different values for λ_u, and fix the bounds

$$\alpha = -10, \quad \beta = 10.$$

  Since $\lambda_T = 0$, only the ratio of λ_u/λ_Q is relevant for the optimization, hence one of the two parameters might be set to one. This is indeed the standard setting in quadratic tracking type funtionals with regularization term. While this is true from an analytic point of view, in the numerical calculations both values have their own right. This is due to possible cancellation of digits.

- *Initial state:* For y_0, we take the constant vector given by the steady state solution y of the system (2.17) that is associated with the constant control $u(t) \equiv 6\,V$, while the initial current i_0 is defined by $i_0 \cdot R_c = 6\,V$. For R_c defined above, this amounts to $i_0 = 0.6\,A$.

- *Numerical solution of the FE system:* As finite elements, we applied H-curl elements with degree $p = 2$ that obey the associated Dirichlet boundary conditions at $\partial\Omega$. For the Crank-Nicolson method in time, the weight 0.5 and the time step size $\tau = 10^{-5}$ were taken to cope with very steep slopes of the optimal voltage. For solving the full discretized Maxwell equations, we invoked the FE code NGSOLVE by J. Schöberl, [21].
  Moreover, we applied an elliptic regularization with the differential operator

$$u \mapsto \operatorname{curl} \mu^{-1} \operatorname{curl} u + \kappa\, u,$$

  where $\kappa = 100$.

Computing the optimal control for the full system is a very time consuming task. To overcome this obstacle, we tested proper orthogonal decomposition (POD), a standard method of model order reduction. We refer to Kunisch and Volkwein [15], [16], Afanasiev and Hinze [1], or Volkwein [22] and to the references cited therein. This method is known to be a reliable tool for reducing the order of many types of linear and nonlinear evolution equations. In particular, it was applied to different versions of the nonlinear heat equation or to the Navier-Stokes equations in the case of moderate Reynolds numbers, to mention only some cases. Due to certain similarities of our evolution Maxwell equations to the standard heat equation, we expected that POD might be useful for our application as well. Our expectation turned out to be correct, because POD was extremely efficient.

In the case of the geometry "tube with coil", 5 POD modes were sufficient to reach high precision. Below, we just present the results by this method and do even not show the optimal solutions of the full optimal control problem. In the figures, we display the optimal solutions to the POD reduced model. They are very close to those of the full model. The application of POD to our Maxwell integro-differential system is discussed in detail in our paper [18].

In Fig. 3.1, we present the optimal voltages and the associated optimal electrical currents for the tube with coil. The optimal control voltage u_{POD}^* starts at the maximal possible voltage $10\,V$ and reaches after some time the value $6\,V$ that holds the current of $0.6\,A$. In the figure, the computed optimal voltage u_{POD}^* is compared with $\mathbb{P}_{[\alpha,\beta]}\left(-q_{POD}^*/\lambda_u\right)$. For the ratio $\lambda_u/\lambda_Q = 10^{-5}$, both functions graphically coincide, hence u_{POD}^* very well satisfies the optimality conditions ("optimality test"). For 10^{-6} and smaller ratios, the optimality test is less satisfactory. Here, λ_u/λ_Q seems to have reached the precision of solving the POD reduced differential equation.

The optimal current i_{POD}^* is presented in Fig. 3.2 for $\lambda_Q = 10^5$ and different values of λ_u. For
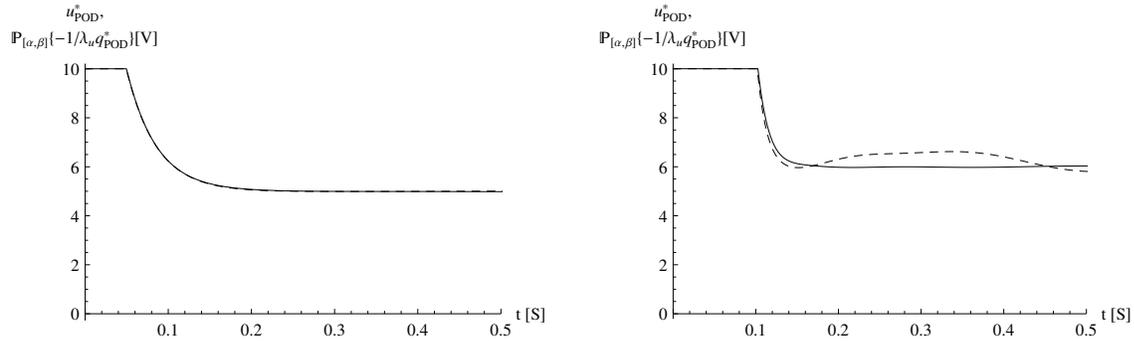
18

FIG. 3.1. *Example 1: Optimal voltage u^*_{POD} compared with $\mathbb{P}_{[\alpha,\beta]}\left(-q^*_{POD}/\lambda_u\right)$ for different ratios λ_u/λ_Q (optimality test). Left hand side: $\lambda_u/\lambda_Q = 10^{-5}$, right hand side: $\lambda_u/\lambda_Q = 10^{-6}$.*
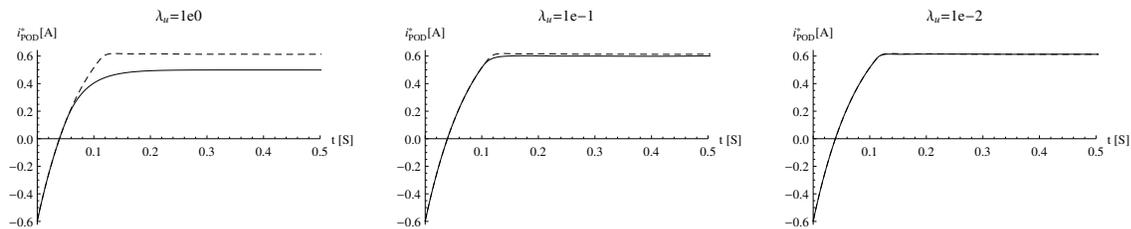

FIG. 3.2. *Example 1: Optimally controlled current i^*_{POD} for $\lambda_Q = 10^5$, $\lambda_u = 1, 0.1, 0.01$, and for $\lambda_u = 0$ (dashed).*

$\lambda_u = 10^{-2}$, the optimal current has the principal form that is to be expected for $\lambda_u = 0$. Starting with $-0.6\,A$, after an initial phase, the current of $0.6\,A$ is reached.

For completeness, in Fig. 3.3 we also show the result for $\lambda_u = 0$. To get an adequate numerical coupling between the forward and adjoint equations we choose λ_Q large enough, 10^5 in the example. Here, to satisfy the necessary optimality conditions, the following complementarity conditions must hold true:

$$q^*_{POD}(t) < 0 \;\Rightarrow\; u^*_{POD}(t) = 0.6 \quad \text{and} \quad -0.6 < u^*_{POD}(t) < 0.6 \;\Rightarrow\; q^*_{POD}(t) = 0. \qquad (3.1)$$

The computed optimal solution obeys these conditions almost perfectly.

3.3. Example 2: Real application and model reduction. In the case of our academic geometries, we were able to apply the projected gradient method to the full finite element discretization of our model, because we selected fairly rough meshes. Moreover, we stopped the method after a small number of gradient steps. In an industrial application to flow measurement, very fine effects are to be measured. Much higher computational precision is required so that a finer FE mesh, very small time steps, and a large number of iterations of the gradient method are needed. Let us explain the consequences for an industrial sensor that is presented in Fig. 3.4.

The FE mesh that we used to solve the Maxwell equations, contained $109\,282$ elements and had $1\,054\,050$ degrees of freedom. To achieve a moderate precision, the state equation was solved
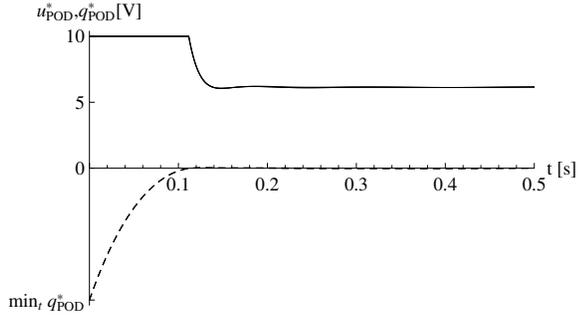
Fig. 3.3. *Example 1: Optimal control u^*_{POD} for $\lambda_Q = 10^5$, $\lambda_u = 0$; comparison with q^*_{POD} (dashed).*
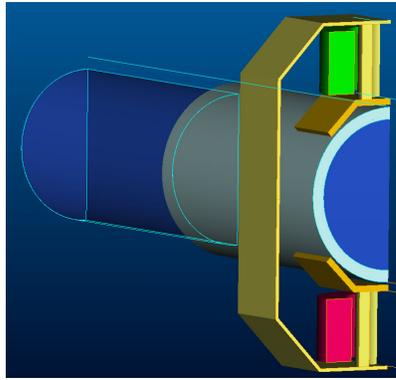

Fig. 3.4. *Example 2: Industrial DN50 Sensor*

with only 200 time steps. For a time horizon of $T = 40\,ms$, this amounts to time steps of length $2 \cdot 10^{-4}\,s$. Under this discretization, solving the state equation by NGSOLVE needs 5.2 hours. In each iteration of the gradient method, we have to solve the state equation and the adjoint equation, hence 10.4 hours are needed for each iteration. To get an acceptable precision, some hundred gradient steps must be performed, say only 100. In this case, the gradient method would take more than 43 days of CPU time. This is certainly not acceptable for industrial applications.

To overcome this obstacle, we again tested POD. For the case of the industrial DN50 sensor, we invoked POD for the FE discretized model explained above. Moreover, we selected 4000 time steps to reach the precision needed for the industrial application. Instead of hours, one solve of the POD reduced state equation took only some milliseconds. Eight POD ansatz functions were sufficient to achieve the required precision. Applied to the optimization of this reduced order model, the projected gradient method takes only a few minutes.

It is not our aim to report on the details of model order reduction here and we refer again to our paper [18]. We have mentioned the setting of the DN50 sensor and the high potential of model reduction to convince the reader that optimal control methods can be efficiently applied to this particular class of problems with real industrial background.

REFERENCES

[1] K. Afanasiev and M. Hinze. Adaptive control of a wake flow using proper orthogonal decomposition. In *Shape Optimization & Optimal Design*, volume 216 of *Lect. Notes in Pure and Appl. Math.*, pages 317–332. Marcel Dekker, 2001.

[2] K. Altmann. *Numerische Verfahren der Optimalsteuerung von Magnetfeldern*. Phd thesis, Technical University of Berlin, 2013.

[3] K. Altmann, S. Stingelin, and F. Tröltzsch. On some optimal control problems for electric circuits. *International Journal of Circuit theory*, 2013, doi: 10.1002/cta.1889.

[4] G. Bärwolff and M. Hinze. Optimization of semiconductor melts. *ZAMM Z. Angew. Math. Mech.*, 86(6):423–437, 2006.

[5] P.E. Druet, O. Klein, J. Sprekels, F. Tröltzsch, and I. Yousept. Optimal control of three-dimensional state-constrained induction heating problems with nonlocal radiation effects. *SIAM J. Control Optim.*, 49(4):1707–1736, 2011.

[6] R. Griesse and K. Kunisch. Optimal control for a stationary MHD system in velocity-current formulation. *SIAM J. Control Optim.*, 45(5):1822–1845, 2006.

[7] M. Gunzburger and C. Trenchea. Analysis and discretization of an optimal control problem for the time-periodic MHD equations. *J. Math. Anal. Appl.*, 308(2):440–466, 2005.

[8] M. Hinze. Control of weakly conductive fluids by near wall Lorentz forces. *GAMM-Mitt.*, 30(1):149–158, 2007.

[9] D. Hömberg and J. Sokołowski. Optimal shape design of inductor coils for surface hardening. *Numer. Funct. Anal. Optim.*, 42:1087–1117, 2003.

[10] L. S. Hou and A. J. Meir. Boundary optimal control of MHD flows. *Appl. Math. Optim.*, 32(2):143–162, 1995.

[11] L. S. Hou and S. S. Ravindran. Computations of boundary optimal control problems for an electrically conducting fluid. *J. Comput. Phys.*, 128(2):319–330, 1996.

[12] D. Kinderlehrer and G. Stampacchia. *An Introduction to Variational Inequalities and their Applications*. Academic Press, New York, 1980.

[13] M. Kolmbauer. *The multiharmonic finite element and boundary element method for simulation and control of eddy current problems*. Phd thesis, 2012.

[14] M. Kolmbauer and U. Langer. A Robust Preconditioned MinRes Solver for Distributed Time-Periodic Eddy Current Optimal Control Problems. *SIAM J. Sci. Comput.*, 34(6):B785–B809, 2012.

[15] K. Kunisch and S. Volkwein. Galerkin proper orthogonal decomposition methods for parabolic problems. *Numer. Math.*, 90(1):117–148, 2001.

[16] K. Kunisch and S. Volkwein. Galerkin proper orthogonal decomposition methods for a general equation in fluid dynamics. *SIAM J. Numerical Analysis*, 40:492–515, 2002.

[17] C. Meyer, P. Philip, and F. Tröltzsch. Optimal control of a semilinear PDE with nonlocal radiation interface conditions. *SIAM J. Control Optimization*, 45:699–721, 2006.

[18] S. Nicaise, S. Stingelin, and F. Tröltzsch. Optimal control and model reduction for two magnetization processes. *To appear in Discrete and Continuous Dynamical Systems*.

[19] S. Nicaise and F. Tröltzsch. A coupled Maxwell integrodifferential model for magnetization processes. *Mathematische Nachrichten*, 2013.

[20] S. S. Ravindran. Real-time computational algorithm for optimal control of an MHD flow system. *SIAM J. Sci. Comput.*, 26(4):1369–1388 (electronic), 2005.

[21] J. Schöberl. NGSolve finite element library. http://sourceforge.net/projects/ngsolve.

[22] S. Volkwein. Model reduction using proper orthogonal decomposition. Lecture notes, Institute of Mathematics and Scientific Computing, University of Graz, 2007.

[23] I. Yousept. Optimal control of Maxwell's equations with regularized state constraints. *Comput. Optim. Appl.*, 52(2):559–581, 2012.

[24] I. Yousept and F. Tröltzsch. PDE-constrained optimization of time-dependent 3d electromagnetic induction heating by alternating voltages. *ESAIM M2AN*, 46:709–729, 2012.